Kinetics of PL Quenching during Single-Walled Carbon Nanotube Rebundling and Diameter-Dependent Surfactant Interactions†

Timothy J. McDonald,*,‡,§ Chaiwat Engtrakul,‡ Marcus Jones,‡ Garry Rumbles,‡ and Michael J. Heben*,‡

Center for Basic Sciences, National Renewable Energy Laboratory, Golden, Colorado 80401, and Department of Applied Physics, Columbia University, New York, New York 10027

Received: August 15, 2006; In Final Form: September 28, 2006

The kinetics of single-walled carbon nanotube rebundling have been investigated by photoluminescence (PL) spectroscopy. The rate of loss of PL intensity was measured for 12 different nanotubes in three common aqueous surfactants (sodium dodecyl sulfate, SDS; sodium dodecylbenzene sulfonate, SDBS; and sodium cholate, SC) as the surfactant suspensions were diluted to promote nanotube rebundling, quenching of semiconductor nanotube PL, and precipitation. The rate of PL decay was first-order in the concentration of isolated nanotubes, as expected if surfactant desorption is rate-limiting in the rebundling process. Temperature-dependent measurements permitted an Arrhenius analysis from which diameter-dependent activation energies were determined. SDS was found to have very strong diameter dependence for activation energy, with stronger binding to smaller-diameter nanotubes, whereas SDBS displayed a weaker diameter dependence. SC was found to bind strongly to certain nanotubes and weakly to the (10,2) nanotube. The PL emission red shifted with time after dilution as surfactant desorption proceeded. This effect is attributed to an increase in the micropolarity at the nanotube surface.

Collections of single-walled carbon nanotubes (SWNTs) with the same physical structure and electronic type are required for many electronic,[1−5] photonic,[6−11] sensor,[12,13] and energy storage and conversion applications.[14−17] Unfortunately, current nanotube synthesis methods typically produce a distribution of metallic and semiconducting nanotubes that have structure-dependent optoelectronic properties.[18,19] The polydispersity in diameter and chirality, and hence in the electronic character, is due to the numerous ways that seamless nanotubes of (*n*,*m*) type can be formed by "rolling-up" the planar graphene lattice.[1,20] In fact, at least 20 unique semiconducting nanotube types are observed in two-dimensional excitation versus emission photoluminescence contour maps (PL contour maps) in both laser[21] and HiPco[22] nanotubes. The total number of nanotubes present is likely 50% larger given that metallic nanotubes, which are nonemissive in photoluminescence (PL) spectroscopy, are present in a ratio of ∼1:2 relative to semiconducting nanotubes. Although significant progress has been made in reducing the dispersity in nanotube type during synthesis,[23,24] more than 100 different types of nanotubes are possible.[25]

As-produced and purified SWNTs are typically tangled and strongly van der Waals bonded to one another in the solid state and, therefore, are difficult to sort. O'Connell et al. employed aggressive sonication in aqueous surfactant solutions to overcome nanotube−nanotube van der Waals interactions and produced stable nanotube colloids that remained suspended after prolonged ultracentrifugation.[11] This advance raised the possibility of sorting nanotubes by diameter and/or conductivity type in solution using a variety of separation techniques. For example, some diameter purification has been achieved by exposing DNA-suspended nanotubes to density gradients[6] and ion-exchange chromatographic columns.[26] Separation according to metallicity has been achieved by exposing surfactant suspended SWNTs to diverging, alternating electric fields.[27] Selective reactions between diazonium salts and surfactant-suspended SWNTs have also been used to separate nanotubes by metallic character.[28,29] Clearly, many of the sorting strategies developed to date seek to capitalize on selective interactions between nanotubes suspended by surfactants in solutions. Unfortunately, very little is known about the nature of these interactions or the degree to which they vary with nanotube diameter, chirality, or, more specifically, (*n*,*m*) indices.

Here, we present measurements of the steady-state PL intensity decay for 12 semiconducting nanotubes as surfactant-stabilized solutions were diluted to promote nanotube rebundling and precipitation. The PL intensity decay displayed first-order kinetics for all nanotubes, as expected if surfactant desorption from the nanotube surfaces is rate-limiting in the rebundling kinetics. The measurements were repeated at several different temperatures, and an Arrhenius analysis yielded E_a, the activation energy for surfactant desorption, for each nanotube in three commonly used surfactants: sodium dodecyl sulfate (SDS), sodium dodecylbenzene sulfonate (SDBS), and sodium cholate (SC). For SDS, E_a was found to vary relatively smoothly by a factor of 6 across the nanotube diameter range, whereas SDBS showed a much weaker dependence of E_a on diameter, varying only by a factor of ∼2. The activation energy for surfactant desorption was largest for the smaller-diameter nanotubes in both cases. Interestingly, E_a for SC deviated strongly from a

† Part of the special issue "Arthur J. Nozik Festschrift".

* Corresponding authors. E-mail: michael_heben@nrel.gov (M.J.H.), tm2008@columbia.edu (T.J.M.).

‡ National Renewable Energy Laboratory.

§ Columbia University.

10.1021/jp065281x CCC: $33.50
Published on Web 11/23/2006

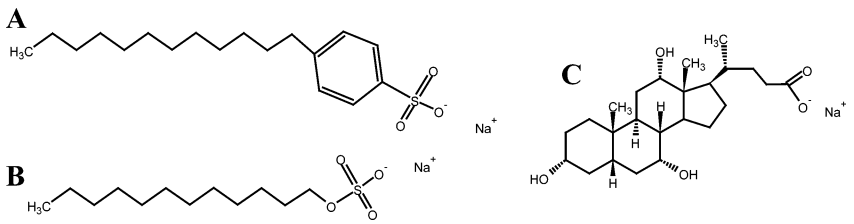

Figure 1. Chemical structures of the three surfactants used in this study: (A) sodium dodecylbenzene sulfonate, (B) sodium dodecyl sulfate, and (C) sodium cholate.

smooth diameter trend, showing a strong preference for certain nanotubes and a very weak binding with the (10,2) nanotube. Under our experimental conditions, the variation in E_a across the nanotube distribution for each surfactant is a measure of the variation of the nanotube−surfactant binding energy. These findings help explain successful nanotube-specific purifications that have been presented in the literature[6,26−29] and point the way toward new bulk purification strategies.

Experimental Section

Purified HiPco SWNTs from Carbon Nanotechnologies Inc.[30] were mixed in aqueous solutions containing 1%, 1%, and 0.3% (wt/wt) of SC, SDS, and SDBS (all from Sigma-Aldrich), respectively. The initial surfactant concentration of SDBS was lower because of its much lower critical micelle concentration (CMC). The chemical structures of the three surfactants are shown in Figure 1. The mixtures were agitated by cup−horn sonication with a Cole Parmer 750 W homogenizer at 30% power for 15 min and then sonicated overnight in a Branson 2510 ultrasonic bath. A final cup−horn sonication at 100% power followed immediately by ultracentrifugation at 122000*g* removed large bundles from the suspension. This process is reported to produce suspensions having single and relatively small bundles of nanotubes that are stabilized against agglomeration by the adsorbed surfactant species.[11] The resulting suspensions were stable for many months without any discernible changes and exhibited photoluminescence from the semiconducting nanotubes in the near-infrared portion of the optical spectrum.

PL contour maps were obtained with a customized Thermo-Electron FT960 Raman system that has been recently described.[31] Briefly, the excitation source of the Raman spectrometer was replaced with a 250-W tungsten halogen bulb and a single-grating monochromator to permit continuously variable excitation from 400 to 1100 nm. The Ge detector, operated at 77 K, responded to wavelengths between 900 and 1700 nm. The system was corrected for variations in excitation intensity as a function of wavelength and for the response of the collection optics and detector. Temperature control of the sample was achieved with a Cole Parmer DigiSense temperature controller connected to a cartridge heater. The heater was in thermal contact with a 1-cm-path-length cuvette mounted in a metallic holder. A thermocouple was immersed in the suspension to monitor the temperature.

Results and Discussion

The PL quenching associated with nanotube rebundling can be seen in the PL contour map for an SWNT suspension in aqueous SDS before and after removal of surfactant. Figure 2A shows the initial PL contour map data for an SWNT suspension in 1 wt % (~35 mM) SDS. Each spot in the PL contour map signals the presence of a particular isolated semiconducting nanotube species in the suspension. Nanotube indices were

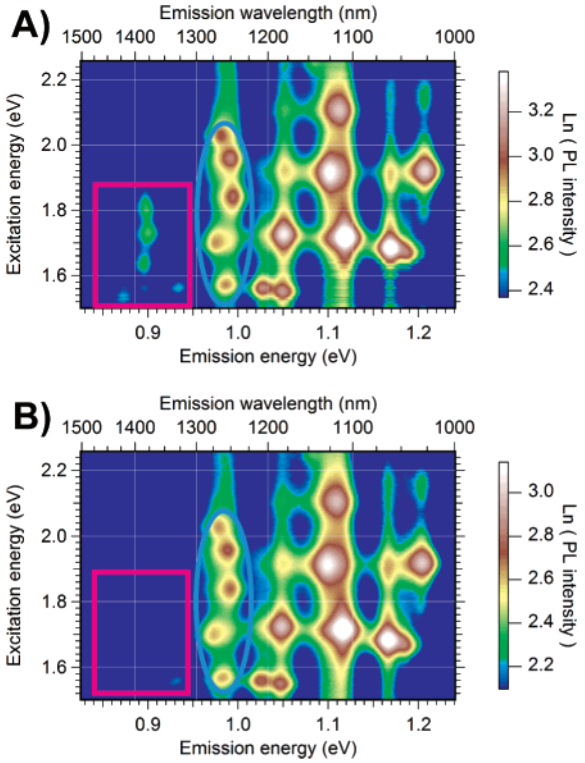

Figure 2. (A) Two-dimensional excitation versus emission photoluminescence contour map (PL contour map) of HiPco SWNTs suspended in 1 wt % SDS surfactant. (B) PL contour map of the same suspension after 2 h of dialysis to remove excess surfactant. Larger nanotube types (generally at lower-energy emission) have been preferentially quenched. The color is proportional to the natural logarithm of PL intensity and is in arbitrary units.

assigned as described by Weisman et al.[32] and Bachilo et al.[22] The suspension was placed in a 3-mL cassette (Pierce Slide-A-Lyzer 3500 MWCO) and dialyzed against 2.5 L of pure water for 2 h. The dialysis reduced the concentration of surfactant in the suspension without diluting the SWNT concentration. After dialysis (Figure 2B), the PL emission from the largest semiconducting nanotubes (those with the lowest emission energy) is absent (Figure 2, pink squares), and the intensity of emission from the next largest set of nanotubes has been noticeably diminished (Figure 2, blue ovals). Because absorption spectroscopy shows that the large-diameter nanotubes are still present in the solution, we can conclude that the PL from these nanotubes has been quenched through nanotube−nanotube interactions promoted by removal of the surfactant. Apparently, the large-diameter nanotubes in the distribution are more susceptible to surfactant loss and, therefore, more likely to interact and rebundle.

Surfactant molecules in SWNT suspensions can be free in solution, assembled into micelles, or adsorbed onto nanotube surfaces.[33] The distribution of surfactant species between these phases is governed by coupled surfactant−water, surfactant−

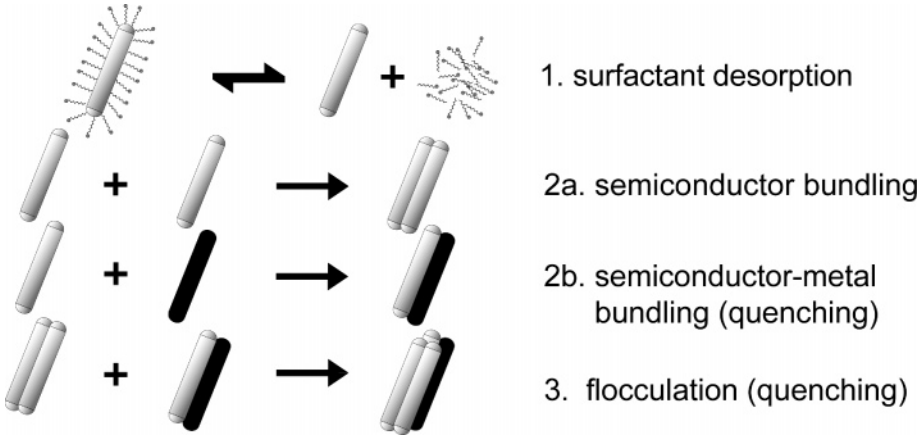

Figure 3. Simplified schematic of steps in nanotube rebundling and flocculation. The gray tubes represent semiconducting nanotubes, and the black tubes represent metallic nanotubes.

surfactant, and nanotube−surfactant equilibria. Nanotubes are stably isolated when nanotube−surfactant interactions are strong relative to surfactant−surfactant and surfactant−water interactions such that surfactant remains adsorbed and prohibits nanotubes from contacting one another and reforming van der Waals-stabilized bundles. In fact, nanotubes in stable aqueous suspensions do not reaggregate until the surfactant concentration is reduced substantially below the CMC.[34]

The quenching of nanotube PL associated with rebundling can be considered using the simplified schematic model shown in Figure 3. Here, nanotube flocculation and subsequent PL quenching is initiated by a surfactant desorption step (step 1). This step is followed by the formation of small bundles that can still remain suspended (step 2). Two semiconducting nanotubes can rebundle (step 2a, gray tubes), and if the two semiconducting nanotubes are of different band gaps, energy transfer can cause partial quenching of the larger-band-gap nanotube.[35] Rebundling of a semiconducting nanotube with a metallic nanotube (step 2b, black tube) quenches the PL from the former.[11] Step 3 is the formation of larger bundles, with further PL quenching and eventual nanotube flocculation and precipitation. In this model, we consider step 1 to be a reversible process because the adsorption of surfactant on graphite and nanotube surfaces is known to be characterized by adsorption isotherms,[28,36] whereas steps 2 and 3 are presumed to be largely irreversible, consistent with the need for probe sonication to overcome van der Waals forces and break up bundles during sample preparation. Although greatly simplified, this model is instructive. For example, the observation that the PL from large-diameter nanotubes is preferentially quenched upon surfactant dilution suggests that the equilibrium constants for step 1 depend on the nanotube diameter.

To study the kinetics of the PL quenching in more detail, we examined SWNT suspensions that were abruptly diluted with pure water. The degree of dilution was selected to reduce the surfactant concentration below the stable nanotube suspension concentration (SNSC). The SNSC for each surfactant was assessed by reducing the surfactant concentration in ∼1 mM steps until decay in the PL intensity could be detected after 2 h at 30 °C. The experimentally determined SNSC values were approximately one-half of the corresponding CMC values. Dilution to concentrations significantly below the SNSC made PL decay measurements difficult to record because of the rapid rebundling process, whereas insufficient dilution led to excessively long experiments. Table 1 reports the pre- and post-dilution surfactant concentrations, as well as the CMCs and SNSCs for the three chosen surfactants. In general, suspensions diluted to surfactant concentrations just below the SNSC slowly flocculated and emitted no observable PL after 2 days at ambient temperature.

TABLE 1: Surfactant Concentrations Used in This Study

surfactant	CMC (25 °C) (mM)	SNSC (30 °C) (mM)	predilution conc (mM)	post-dilution conc (mM)
SDS	8.35	3.6	34.67	3.15
SDBS	1.6	0.8	8.61	0.54
cholate	∼6	2.3	23.23	0.93

To monitor the time dependence of the PL from all detectable semiconducting nanotubes, we first measured a PL contour map like the one shown in Figure 2 and identified the peak excitation wavelengths for each semiconducting nanotube. The excitation monochromator was then rapidly stepped between the peak excitation wavelengths to increase the data acquisition rate and enable the PL from all observable nanotubes to be measured every few minutes. More thorough PL contour map scans were occasionally performed to ensure that the peak excitation wavelengths did not vary substantially through the course of the experiments.

Figure 4A shows the PL decay kinetics for three representative nanotube species in an SDBS solution at 40 °C after dilution to a surfactant concentration below the SNSC (Table 1). The data clearly show different PL decay rates for the three different nanotubes, each with a different quenching constant, *k*. The oscillation in the data points around the fit line (vide infra) is likely associated with imperfect temperature control during the course of the experiment.

Figure 4B shows the decay in PL intensity for the (9,4) nanotube at three different temperatures and demonstrates that the PL quenching is strongly thermally activated. The data in Figure 4C show the PL quenching kinetics for the (9,4) nanotube at 40 °C in solutions containing the three different surfactants. In this comparison, we find that the quenching rates for the SC- and SDBS-suspended (9,4) nanotubes are quite similar, whereas the quenching rate for SDS is significantly higher. This result is surprising considering that SDS and SDBS are both "classic" molecular surfactants in that they both have polar headgroups and symmetric nonpolar tails and differ only by the presence of a benzene ring, whereas SC is asymmetric (Figure 1). Previous reports have shown that SC suspensions have better-resolved absorption transitions and brighter PL than similarly prepared SDS suspensions.[37]

Surprisingly, all of the PL decay data are well-fit by the integrated form of a first-order rate equation that describes the PL intensity decay for the *i*th nanotube species from its initial

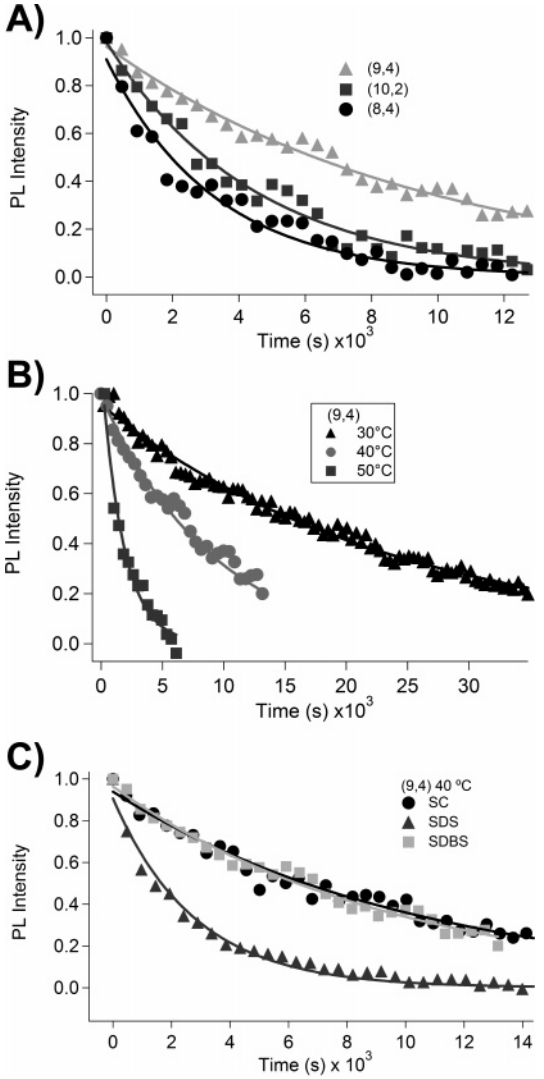

Figure 4. Photoluminescence intensity maximum versus time for (A) an SDBS suspension for three different nanotube species, (B) an SDBS suspension for a single nanotube species at three different temperatures, and (C) the (9,4) nanotube suspended in three different surfactants.

value, I_{i0}, as a function of time, t, with a characteristic rate constant, $k_i(T)$, at each temperature, T (lines in Figure 4).

$$\frac{I_i}{I_{i0}} = \exp[-k_i(T)\cdot t] \qquad (1)$$

This is understood within the context of the model of Figure 3 by considering the PL intensity to be a measure of the concentration of isolated semiconductor SWNTs and step 1 in Figure 3 to be the rate-determining step in the quenching process. Before dilution the surfactant concentration is substantially higher than the CMC and surfactant molecules are present free in solution, assembled into micelles, and bound to the nanotube surface. After dilution, the surfactant concentration is reduced by a factor of 10−25 and the dynamic SWNT−surfactant equilibrium shifts to the right. Surfactant species desorb from the SWNT surfaces to reestablish equilibrium leaving partially unsheathed nanotubes that can readily rebundle. Consistent with a thermally activated process, the rate of PL quenching is increased at higher temperatures as seen in Figure 4B. We note that the temperature range in this experiment is small enough that the quantum yield can be considered constant as the temperature is raised.[38] Theoretical[39] and experimental[40]

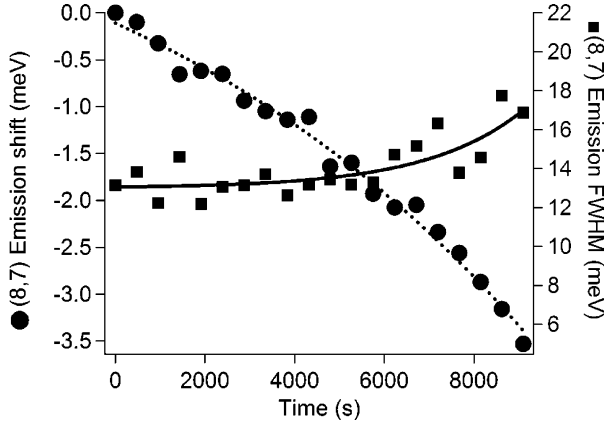

Figure 5. Full width at half-maximum (fwhm) and emission red shift for the (8,7) nanotube in SDS suspension at 50 °C after dilution (Table 1).

studies show that the van der Waals binding between SWNTs is quite strong, with as much a 2.5 eV per nanometer of contact length for nanotubes of the same diameter range as those used here. Thus, rapid rebundling (step 2, Figure 3) is expected when bare or partially bare nanotube surfaces come into contact with one another. The ability to fit the data with a first-order rate expression suggests that the rebundling reactions are fast relative to step 1 and that the surfactant desorption step is rate-limiting. In contrast, if a combination of steps 2 and 3 were rate-limiting in the PL quenching, one would expect kinetics that reflected a component that was second-order in the concentration of luminescent nanotubes, which is not observed. We note that a first-order rate description is valid for all nanotubes, at all temperatures, for each surfactant.

Whereas first-order kinetics provide a good fit to the data and indicate that step 1 is rate-determining, the PL emission is also observed to red shift slightly during rebundling. This finding suggests that step 2 in our model (Figure 3), which is bundling of semiconducting nanotubes, might be measured as imparting a red shift in the electronic transitions of each nanotube.[41,42] Figure 5 shows the emission peak position and line width (fwhm) as a function of time for the (8,7) nanotube in SDS after dilution at 50 °C (Table 1). A red shift of 3.5 meV is observed over the course of the 3.5-h experiment. The emission feature line-width remains relatively constant at 13.5 meV until late in the experiment, at which time the emission peak broadens slightly to ∼17 meV. The values were extracted from the data by fitting Lorentzian functions to the emission features,[43] and similar behavior was observed for all nanotube−surfactant combinations.

Reich et al. calculated a red shift of ∼100 meV in the transition energies of roped versus isolated nanotubes,[44] whereas Raman spectroscopy has shown that transition energies for roped nanotubes in the solid state are reduced by 20−157 meV with respect to those of SDS-suspended nanotubes.[45] The red shifts we observe are small in comparison, presumably because our experiments monitor the initial stages of bundling. More complete bundling would quench the PL and not be observable in our experiments. Recent Rayleigh scattering experiments by Wang et al. showed that the transition energies for nanotubes in two-tube bundles are red shifted by a only few tens of millielectron volts relative to those of the individual nanotubes.[41] The spectral changes are ascribed to mutual dielectric screening effects. Interestingly, the transition widths measured by Wang et al. were unaltered in the small bundles, in good agreement with our observations in Figure 5. However, if spectral changes associated with nanotube−nanotube contact were being observed

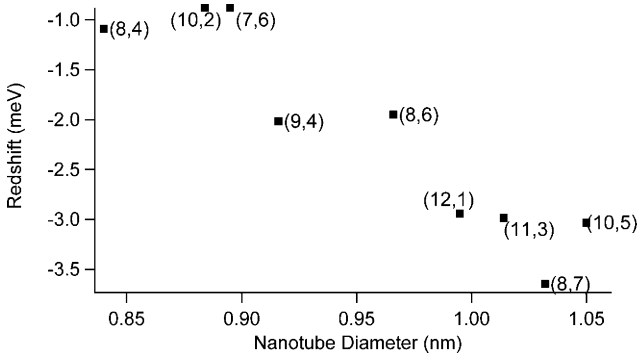

Figure 6. Red shift of PL emission peak wavelength for nine different nanotube types versus tube diameter for a diluted SDS suspension after 150 min.

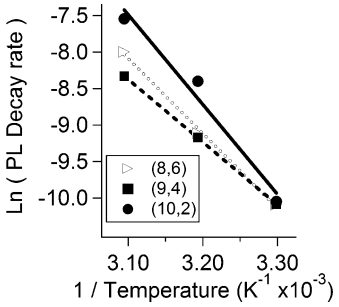

Figure 7. Points: Natural logarithm of PL decay rate after dilution for three semiconducting nanotube species versus inverse temperature in SDBS. Lines: Linear function fit to the data, the slope of which determines the activation energy for the PL quench for each nanotube type.

in our experiments, an increase in the emission fwhm over time would be expected since many different types of small bundles and isolated nanotubes contributed to the emission signal.

Strano et al. investigated changes to the Raman and PL properties of constantly sonicated SWNT suspensions as SDS was added to the mixture.[34] The concentration of isolated SWNTs, as detected by PL, increased with each addition of surfactant with a time constant of between 20 min and 1 h. Interestingly, an ~8 meV blue shift in the PL from specific nanotubes was seen immediately upon addition of SDS. The behavior was explained by considering that added surfactant rapidly adsorbed onto already-isolated nanotubes and excluded water such that the micropolarity at the nanotube/solution interface was decreased.[34,46] The initial shift was seen to relax after the first surfactant additions, presumably because of a reduction in the surfactant coverage per nanotube as new nanotubes were brought into solution and surfactant was dynamically reallocated. Despite the fact that these experiments considered dispersion of nanotubes whereas ours deal with rebundling, the spectral shifts in the PL are comparable. The rapid surfactant adsorption observed by Strano et al.[34] versus the slow surfactant desorption reported here is readily explained by considering the former to be energetically downhill whereas the latter requires thermal activation. Similarly, Huang et al. observed a red shift in the emission from nanotubes with reduced surfactant concentrations.[42]

Figure 6 shows a plot of the magnitude of the emission red shift for several nanotube species 150 min after dilution. The magnitude of the red shift scales with the diameter of the nanotube. Following the idea that the red shift is due to increased accessibility of water to the nanotube surface, we conclude that the surfactant coverage is less complete and more weakly adsorbed for the larger-diameter nanotubes, consistent with the data presented in Figure 3.

The activation energy (E_a) associated with the first-order PL decay process can be evaluated from the temperature dependence of the rate constants for each nanotube and surfactant. Figure 7 shows an Arrhenius plot of $\ln k_i(T)$ versus $1/T$ for three specific nanotubes in an SDBS suspension. A straight line produces a good fit to the data and yields a slope of $-E_a/k_B$, where k_B is Boltzmann's constant. Figure 8 shows the E_a values for all of the nanotubes investigated, for each surfactant, as a function of diameter. The SDS data scale smoothly by a factor of ~6 with nanotube diameter, whereas SDBS shows less than a factor of 2 variation across the same range. The surfactant desorption activation energy for the smaller-diameter nanotubes is higher in both cases. The larger diameter dependence seen for SDS is consistent with the report from Okazaki et al. showing that SDS preferentially suspends smaller-diameter nanotubes whereas SDBS suspends all diameters equally well.[47] Interestingly, the measured activation energies are, on average across diameter, not too far from the heats of adsorption of sodium *n*-decyl sulfate (42 kJ mol^{-1}) and dodecyltrimethylammonium bromide (C_{12}-TAB) (61 kJ mol^{-1}) on planar graphite as measured by calorimetric techniques.[36,48] Note that the SDBS and SDS data exhibit a relatively small deviation from the straight-line fit, whereas the trend for the SC values with diameter is not smooth. For example, E_a for the (7,5) nanotube in SC is 10 times that of the (10,2) nanotube even though the nanotube diameters differ by only 0.55 Å (Figure 8 and Table 2). Thus, depending on the surfactant, there is a general relationship between decreasing diameter and increasing E_a as well as highly specific interactions with specific nanotubes.

It is interesting to consider how the surfactant surface density changes with dilution. The predilution surfactant concentrations were 4−5 times higher than the CMCs and 10 times larger than the SNSCs, whereas post-dilution concentrations were substantially less than the SNSCs (Table 1). For comparison with our results, we considered a study by Matarredona and et al. on the adsorption behavior of SDBS on populations of SWNTs.[49] Although nanotube-specific data were not obtained, the maximum coverage of SDBS on SWNTs was measured to occur at concentrations greater than ~3.4 mM. The adsorbed amount was reduced by almost 2 orders of magnitude when the concentration was reduced to 0.5 mM. Thus, the concentration change employed in our studies (from 8.61 to 0.54 mM) would reduce the coverage of SDBS from complete saturation to a sparse population.

The depopulation of surfactant from the nanotube's surface occurs into a solution having very little free SDBS; therefore, it is tempting to equate the measured activation energies with surfactant−nanotube binding energies. However, the kinetic relationship between the PL decay rate and the true binding energies also depends on the density of the surfactant coverage and the three-dimensional packing. Reference to the structures of the three different surfactants investigated here (Figure 1) suggests that the molecular surface densities on the nanotubes will be quite different. These considerations explain why the activation energies for SC are lower on average than those for SDS and SDBS despite the fact that SC typically suspends higher concentrations of SWNTs. Nevertheless, we can still conclude that the activation energy trends observed are proportional to the binding energies across the nanotube distribution for a given surfactant.

The nanotube-specific surfactant interactions depend on the details of how the molecular species are in contact and organized

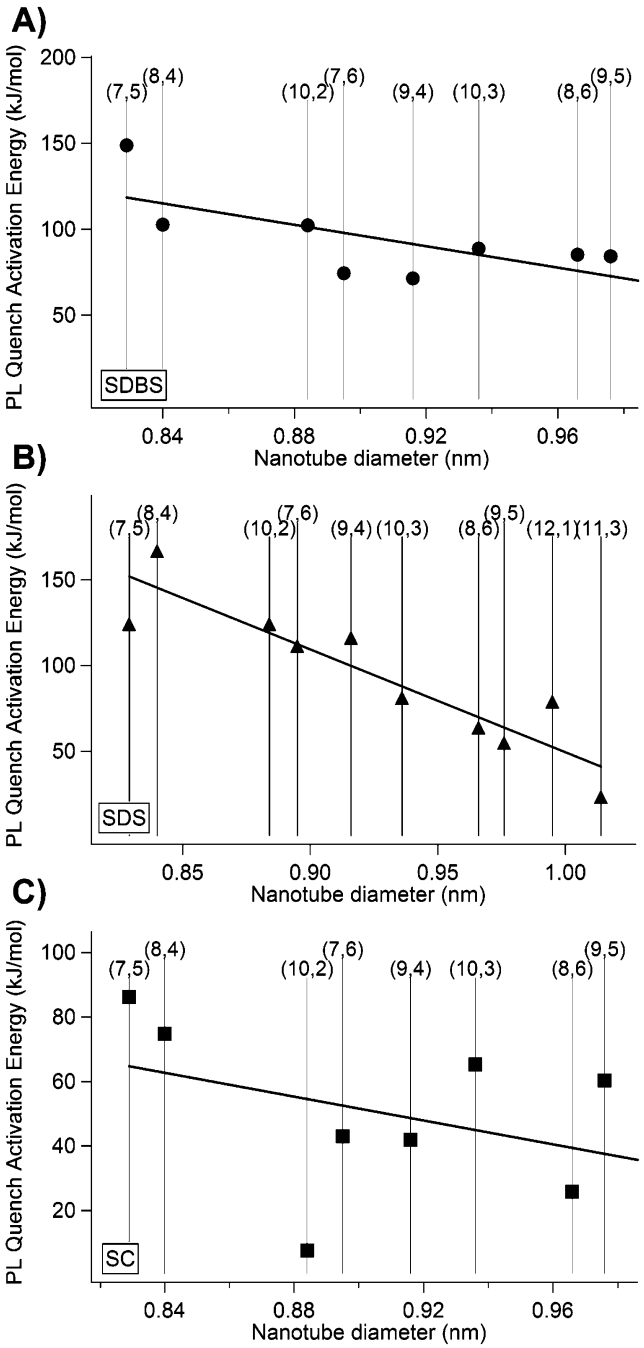

Figure 8. Points: Measured PL quench activation energy versus nanotube diameter for three aqueous surfactants. The standard deviation from the linear fit for (A) SDBS is 19.4 kJ/mol, (B) SDS is 18.4 kJ/mol, and (C) SC is 57.7 kJ/mol.

at the nanotube interface, as well as how the surfactant molecules pack in any extended sheath that might be present. Initial studies using axially symmetric surfactants considered nanotubes to be suspended within the core of a cylindrical micelle,[11] whereas subsequent studies considered the accumulation and organization of surfactant as the adsorbed density was increased.[49−51] At low density, a "head-to-tail" surface phase was postulated in which the long axis of the surfactant was parallel to the nanotube axis, in similarity to surfactant adsorption on planar graphite. Following the analogy to graphite,[36] hemispherical agglomerates were presumed to form with increasing density, with saturation coverage producing cylindrical structures. The formation of cylindrically organized structures templated by the nanotube

TABLE 2: Comparison of PL Quench Activation Energies of Three Aqueous Surfactants with Various Nanotube Types

		E_a[a] (kJ/mol)		
nanotube index (n,m)	diameter (nm)	SDS	SDBS	SC
(7,5)	0.829	124.1	148.8	86.2
(8,4)	0.840	166.8	102.6	74.8
(10,2)	0.884	124.1	102.3	7.6
(7,6)	0.895	111.3	74.4	43.0
(9,4)	0.916	116.0	71.4	41.9
(10,3)	0.936	81.1	88.8	65.3
(8,6)	0.966	63.7	85.2	25.8
(9,5)	0.976	54.8	84.3	60.3
(12,1)	0.995	78.9	NR[b]	NR
(11,3)	1.014	23.3	NR	NR

[a] E_a = PL quench activation energy. [b] NR = not resolved in the spectra.

surface is supported by adsorption isotherm data, which showed that 8 times more surfactant per unit surface area could be accommodated on a nanotube surface as compared to planar graphite.[49] Presumably, the curved nanotube surface permitted a higher-density "tails-on" configuration that offered more space and less repulsion between the polar headgroups. This explanation can be extended to explain the diameter dependence of the surfactant binding seen in our data. Accordingly, smaller-diameter nanotubes would permit a higher packing density of the surfactant tails and less electrostatic repulsion between headgroups. The net effect would be stronger surfactant stabilization for the smaller-diameter nanotubes, as observed. In this case, the weaker dependence of E_a on diameter for the SDBS surfactant can be rationalized if the energy reduction associated with separating the headgroup is smaller for SDBS because of attractive interactions between the benzene rings.

Although conceptually appealing, this explanation for the observed diameter dependence of E_a might be oversimplified even in the case of axially symmetric surfactants. Yurekli et al. probed the structure of SDS adsorbed on nanotubes by small-angle neutron scattering[52] and saw no evidence for the organized surfactant structures that have been presumed. Transmission electron microscopy studies did see organization of SDS on larger-diameter multiwalled nanotubes, but a large variation in the surfactant structures was found.[51] If adsorbed surfactants are not arranged strictly in a tails-on configuration, then some portion of the tail's length will be in contact with the wall of the nanotube. The van der Waals stabilization energy associated with a length (or area) of contacting tail will depend on the degree of commensuration with the nanotube's lattice, which will, in turn, depend on the nanotube's chirality and diameter as well as the relative orientations of the surfactant and nanotube. Furthermore, the energetics of the adsorbed phase will change as a function of solution surfactant concentration and surface packing density. These details might give rise to the nanotube-specific deviations from the straight-line fit in the SDS and SDBS data (Figure 8). Note that we do not expect any role for functional groups that might have been introduced during sample preparation because electronic transitions associated with PL are typically destroyed in covalently functionalized SWNTs.[53]

Clearly, the nanotube-dependent binding becomes more complex for surfactants that are asymmetric or have localized charges in low-symmetry locations. Our measurements show that the activation energies for SC desorption vary widely from an overall weak diameter dependence. The standard deviation from the linear fit across diameter is 57.7 kJ/mol, whereas, for comparison, the deviations for SDS and SDBS are 18.4 and

19.4 kJ/mol, respectively. Surprisingly, the (10,2) nanotube shows an E_a value of only 7.6 kJ/mol, which is more than 50 kJ/mol below the straight-line fit to the diameter dependence. Note that the (10,2) nanotube is not at the large end of the diameter distribution, where the diameter dependence would give rise to weaker binding, but is instead in the middle of the distribution. Thus, it is clear that SC does a very poor job stabilizing the (10,2) nanotube, whereas neighboring (8,4) and (7,6) nanotubes are stabilized with E_a values that are at least 6 times larger. We can consider that the (8,4) and (7,6) nanotubes are "nearly armchair" in configuration and the (10,2) nanotubes are "nearly zigzag", but at the present time, we are unable to articulate a specific geometric relationship between SC and the three nanotube species that could account for strong binding for the (8,4) and (7,6) nanotubes and weak binding for the (10, 2) species.

With these phenomenological observations, it is possible to devise strategies for separating nanotubes from one another in solution. For example, selective precipitation of large-diameter species can leave a solution enriched in small-diameter species (e.g., as in Figure 2). In fact, our findings are fully consistent with the recent chromatographic purification of the (6,5) nanotube by Zheng et al., which was achieved using DNA as a surfactant.[26] Examples of other such purifications will be described in future publications.

In conclusion, we have demonstrated that surfactant desorption from suspended nanotubes is rate-limiting in the rebundling process and that the PL quenching due to bundling is first-order in the concentration of luminescent nanotubes. A relatively smooth diameter dependence exists for the desorption activation energy for symmetric surfactants such as SDS and SDBS, with smaller-diameter nanotubes exhibiting a higher activation energy in both cases. SC, on the other hand, shows a nanotube-specific binding superimposed on a weak diameter dependence that is suggestive of chemical interactions with certain (*n*,*m*) species. A red shift in the emission is interpreted as being due to an improved accessibility of water to the nanotube surfaces as the surfactant coating becomes less dense. A detailed understanding of the geometric and charge-transfer effects that give rise to specific interactions (or lack thereof) is still required so that techniques can be developed to sort nanotubes by (*n*,*m*) type. Ideally, a surfactant "tool kit" would be developed so that species-pure solutions could be obtained in a straightforward manner from polydisperse, as-produced materials. Work toward this goal is continuing in our laboratory.

Acknowledgment. The authors thank Randy Ellingson and Thomas Gennett for helpful discussions. The U.S. Department of Energy (DOE) Solar Photochemistry program funded by the Office of Science, Office of Basic Energy Sciences, Division of Chemical Sciences, Geosciences, and Biosciences supported this work.

References and Notes

(1) Saito, R.; Fujita, M.; Dresselhaus, G.; Dresselhaus, M. S. *Phys. Rev. B* **1992**, *46*, 1804.

(2) Bachtold, A.; Hadley, P.; Nakanishi, T.; Dekker, C. *Science* **2001**, *294*, 1317.

(3) Derycke, V.; Martel, R.; Appenzeller, J.; Avouris, P. *Nano Lett.* **2001**, *1*, 453.

(4) Javey, A.; Guo, J.; Wang, Q.; Lundstrom, M.; Dai, H. J. *Nature (London)* **2003**, *424*, 654.

(5) Wind, S. J.; Appenzeller, J.; Martel, R.; Derycke, V.; Avouris, P. *Appl. Phys. Lett.* **2002**, *80*, 3817.

(6) Arnold, M. S.; Stupp, S. I.; Hersam, M. C. *Nano Lett.* **2005**, *5*, 713.

(7) Arnold, M. S.; Sharping, J. E.; Stupp, S. I.; Kumar, P.; Hersam, M. C. *Nano Lett.* **2003**, *3*, 1549.

(8) Misewich, J. A.; Martel, R.; Avouris, P.; Tsang, J. C.; Heinze, S.; Tersoff, J. *Science* **2003**, *300*, 783.

(9) Wu, Z. C.; Chen, Z. H.; Du, X.; Logan, J. M.; Sippel, J.; Nikolou, M.; Kamaras, K.; Reynolds, J. R.; Tanner, D. B.; Hebard, A. F.; Rinzler, A. G. *Science* **2004**, *305*, 1273.

(10) Freitag, M.; Martin, Y.; Misewich, J. A.; Martel, R.; Avouris, P. *Nano Lett.* **2003**, *3*, 1067.

(11) O'Connell, M. J.; Bachilo, S. M.; Huffman, C. B.; Moore, V. C.; Strano, M. S.; Haroz, E. H.; Rialon, K. L.; Boul, P. J.; Noon, W. H.; Kittrell, C.; Ma, J. P.; Hauge, R. H.; Weisman, R. B.; Smalley, R. E. *Science* **2002**, *297*, 593.

(12) Star, A. J., V.; Han, T. R.; Altoe, M. V. P.; Gruner, G.; Stoddart, F. J. *Org. Lett.* **2004**, *6*, 2089.

(13) Chen, R. J.; Bangsaruntip, S.; Drouvalakis, K. A.; Kam, N. W. S.; Shim, M.; Li, Y. M.; Kim, W.; Utz, P. J.; Dai, H. J. *Proc. Natl. Acad. Sci. U.S.A.* **2003**, *100*, 4984.

(14) Cheng, H.; Yang, Q.Liu, C. *Carbon* **2001**, *39*, 1447.

(15) Kai, S.; Huifang, X.; Yingbin, J.; Tanja Pietra, B. *Carbon* **2004**, *42*, 2315.

(16) van de Lagemaat, J.; Barnes, T. M.; Rumbles, G.; Shaheen, S. E.; Coutts, T. J.; Weeks, C.; Levitsky, I.; Peltola, J.; Glatkowski, P. *Appl. Phys. Lett.* **2006**, *88*, 233503.

(17) Stewart, D. A.; Leonard, F. *Phys. Rev. Lett.* **2004**, *93*, 107401.

(18) Iijima, S.; Ichihashi, T. *Nature (London)* **1993**, *363*, 603.

(19) Haddon, R. C.; Sippel, J.; Rinzler, A. G.; Papadimitrakopoulos, F. *MRS Bull.* **2004**, *29*, 252.

(20) Odom, T. W.; Huang, J. L.; Kim, P.; Lieber, C. M. *J. Phys. Chem. B* **2000**, *104*, 2794.

(21) Lebedkin, S.; Arnold, K.; Hennrich, F.; Krupke, R.; Renker, B.; Kappes, M. M. *New J. Phys.* **2003**, *5*, 140.

(22) Bachilo, S. M.; Strano, M. S.; Kittrell, C.; Hauge, R. H.; Smalley, R. E.; Weisman, R. B. *Science* **2002**, *298*, 2361.

(23) Bachilo, S. M.; Balzano, L.; Herrera, J. E.; Pompeo, F.; Resasco, D. E.; Weisman, R. B. *J. Am. Chem. Soc.* **2003**, *125*, 11186.

(24) Okazaki, T.; Saito, T.; Matsuura, K.; Ohshima, S.; Yumura, M.; Oyama, Y.; Saito, R.; Iijima, S. *Chem. Phys.Lett.* **2006**, *420*, 286.

(25) Weisman, R. B.; Bachilo, S. M.; Strano, M. S.; Kittrell, C.; Hauge, R. H.; Smalley, R. E. *AIP Conf. Proc.* **2003**, no. 685, 241.

(26) Zheng, M.; Jagota, A.; Strano, M. S.; Santos, A. P.; Barone, P.; Chou, S. G.; Diner, B. A.; Dresselhaus, M. S.; McLean, R. S.; Onoa, G. B.; Samsonidze, G. G.; Semke, E. D.; Usrey, M.; Walls, D. J. *Science* **2003**, *302*, 1545.

(27) Krupke, R.; Linden, S.; Rapp, M.; Hennrich, F. *Adv. Mater.* **2006**, *18*, 1468.

(28) Strano, M. S. *J. Am. Chem. Soc.* **2003**, *125*, 16148.

(29) Usrey, M. L.; Lippmann, E. S.; Strano, M. S. *J. Am. Chem. Soc.* **2005**, *127*, 16129.

(30) Bronikowski, M. J.; Willis, P. A.; Colbert, D. T.; Smith, K. A.; Smalley, R. E. *J. Vac. Sci. Technol. A: Vac. Surf. Films* **2001**, *19*, 1800.

(31) McDonald, T. J.; Jones, M.; Engtrakul, C.; Ellingson, R. J.; Rumbles, G.; Heben, M. J. *Rev. Sci. Instrum.* **2006**, *77*, 053104.

(32) Weisman, R. B.; Bachilo, S. M. *Nano Lett.* **2003**, *3*, 1235.

(33) Wang, H.; Zhou, W.; Ho, D. L.; Winey, K. I.; Fischer, J. E.; Glinka, C. J.; Hobbie, E. K. *Nano Lett.* **2004**, *4*, 1789.

(34) Strano, M. S.; Moore, V. C.; Miller, M. K.; Allen, M. J.; Haroz, E. H.; Kittrell, C.; Hauge, R. H.; Smalley, R. E. *J. Nanosci. Nanotechnol.* **2003**, *3*, 81.

(35) Jiang, J.; Saito, R.; Gruneis, A.; Chou, S. G.; Samsonidze, G. G.; Jorio, A.; Dresselhaus, G.; Dresselhaus, M. S. *Phys. Rev. B* **2005**, *71*, 045417.

(36) Kiraly, Z.; Findenegg, G. H.; Klumpp, E.; Schlimper, H.; Dekany, I. *Langmuir* **2001**, *17*, 2420.

(37) Wenseleers, W.; Vlasov, I. I.; Goovaerts, E.; Obraztsova, E. D.; Lobach, A. S.; Bouwen, A. *Adv. Funct. Mater.* **2004**, *14*, 1105.

(38) Lefebvre, J.; Finnie, P.; Homma, Y. *Phys. Rev. B* **2004**, *70*, 045419.

(39) Girifalco, L. A.; Hodak, M.; Lee, R. S. *Phys. Rev. B* **2000**, *62*, 13104.

(40) Chen, B.; Gao, M.; Zuo, J. M.; Qu, S.; Liu, B.; Huang, Y. *Appl. Phys. Lett.* **2003**, *83*, 3570.

(41) Wang, F.; Sfeir, M. Y.; Huang, L.; Huang, X. M. H.; Wu, Y.; Kim, J.; Hone, J.; O'Brien, S. P.; Brus, L. E.; Heinz, T. F. *Phys. Rev. Lett.* **2006**, *96*, 167401.

(42) Huang, H.; Kajiura, H.; Maruyama, R.; Kadono, K.; Noda, K. *J. Phys. Chem. B* **2006**, *110*, 4686.

(43) Jones, M.; Engtrakul, C.; Metzger, W. K.; Ellingson, R. J.; Nozik, A. J.; Heben, M. J.; Rumbles, G. *Phys. Rev. B* **2005**, *71*, 115426.

(44) Reich, S.; Thomsen, C.; Ordejon, P. *Phys. Rev. B* **2002**, *65*, 155411

(45) Fantini, C.; Jorio, A.; Souza, M.; Strano, M. S.; Dresselhaus, M. S.; Pimenta, M. A. *Phys. Rev. Lett.* **2004**, *93*, 147406.

(46) Moore, V. C.; Strano, M. S.; Haroz, E. H.; Hauge, R. H.; Smalley, R. E.; Schmidt, J.; Talmon, Y. *Nano Lett.* **2003**, *3*, 1379.

(47) Okazaki, T.; Saito, T.; Matsuura, K.; Ohshima, S.; Yumura, M.; Iijima, S. *Nano Lett.* **2005**, *5*, 2618.
(48) Kiraly, Z.; Findenegg, G. H. *J. Phys. Chem. B* **1998**, *102*, 1203.
(49) Matarredona, O.; Rhoads, H.; Li, Z.; Harwell, J. H.; Balzano, L.; Resasco, D. E. *J. Phys. Chem. B* **2003**, *107*, 13357.
(50) Islam, M. F.; Rojas, E.; Bergey, D. M.; Johnson, A. T.; Yodh, A. G. *Nano Lett.* **2003**, *3*, 269.
(51) Richard, C.; Balavoine, F.; Schultz, P.; Ebbesen, T. W.; Mioskowski, C. *Science* **2003**, *300*, 775.
(52) Yurekli, K.; Mitchell, C. A.; Krishnamoorti, R. *J. Am. Chem. Soc.* **2004**, *126*, 9902.
(53) Zhao, J.; Park, H.; Han, J.; Lu, J. P. *J. Phys. Chem. B* **2004**, *108*, 4227.